

Experimental demonstration of entanglement pumping with bosonic logical qubits

Jie Zhou,^{1,*} Chuanlong Ma,^{1,*} Yifang Xu,¹ Weizhou Cai,² Hongwei Huang,¹ Lida Sun,¹ Guangming Xue,^{3,4} Ziyue Hua,¹ Haifeng Yu,^{3,4} Weiting Wang,^{1,†} Chang-Ling Zou,^{2,4,‡} and Luyan Sun^{1,4,§}

¹Center for Quantum Information, Institute for Interdisciplinary Information Sciences, Tsinghua University, Beijing 100084, China

²CAS Key Laboratory of Quantum Information, University of Science and Technology of China, Hefei 230026, China

³Beijing Academy of Quantum Information Sciences, Beijing, China

⁴Hefei National Laboratory, Hefei 230088, China

Entanglement is crucial for quantum networks and computation, yet maintaining high-fidelity entangled quantum states is hindered by decoherence and resource-intensive purification methods. Here, we experimentally demonstrate entanglement pumping, utilizing bosonic quantum error correction (QEC) codes as long-coherence-time storage qubits. By repetitively generating entanglement with short-coherence-time qubits and injecting it into QEC-protected logical qubits, our approach effectively preserves entanglement. Through error-detection to discard error states and entanglement pumping to mitigate errors within the code space, we extend the lifespan of entangled logical qubits by nearly 50% compared to the case without entanglement pumping. This work highlights the potential of bosonic logical qubits for scalable quantum networks and introduces a novel paradigm for efficient entanglement management.

Introduction. - Entanglement plays a pivotal role in quantum physics, not only enhancing our understanding of quantum mechanics [1–3] but also serving as a foundational resource for crucial applications such as quantum computation [4], quantum teleportation [5–7], quantum sensing [8, 9], and quantum networks [10, 11]. The creation and maintenance of high-fidelity entangled states between non-local nodes are of substantial significance for the advancement of these technologies. However, the preparation and lifespan of entangled states are often compromised by factors such as decoherence of qubits, noisy transmission channels, and imperfect measurements and gate operations [12, 13]. Traditional methods to enhance entanglement fidelity, such as entanglement purification protocols [14–19], are highly resource-intensive and require the consumption of large numbers of entangled pairs, posing significant experimental challenges. Moreover, interfaces between imperfect entangled pairs and communication channels typically suffer from reduced lifetimes due to the need for rapid interactions and higher entanglement generation rates [20, 21], further limiting the scalability and efficiency of quantum networks.

To address the challenges of resource consumption and entanglement lifetime, innovative strategies are required. One promising approach involves the use of quantum error correction (QEC) codes within local nodes to create long-coherence-time storage qubits [13, 22–26]. By encoding physical qubits into logical qubits, specific types of errors can be detected and corrected, thereby extending the coherence time and enhancing entanglement fidelity. Additionally, employing entanglement pumping (EP) [20, 27]—a more efficient form of entanglement purification—allows for the continuous generation of partially entangled pairs, which are then used to reinforce the entanglement between long-lived storage qubits. This approach reduces resource requirements by utilizing a minimal number of qubits to maintain entangled pairs, as opposed to traditional entanglement purification which consumes exponentially many pairs. The combination of QEC-enhanced storage and EP offers a robust solution for sustaining entanglement

in quantum networks, facilitating more efficient and scalable quantum communication and computation by continuously injecting entanglement resources and mitigating errors within the code space.

In this Letter, we experimentally demonstrate the first implementation of EP applied to logical qubits protected by QEC. By integrating QEC codes as long-coherence-time storage qubits with a repetitive entanglement generation scheme, our EP protocol effectively suppresses decoherence through quantum error detection (ED). Through post-selection, our method discards states that transition into error spaces, while the EP mechanism mitigates errors within the code space, thereby synergistically extending the lifespan of entangled logical qubits (ELQs). Our experimental results show that the application of both EP and ED strategies extends the lifespan of ELQs by nearly 50% compared to using only ED. These findings underscore the potential of bosonic logical qubits [28, 29] in quantum networks and introduce EP as a novel and efficient paradigm for entanglement management. This advancement offers significant implications for the development of reliable and scalable quantum communication and distributed computation systems [30–34], providing new insights into the optimization of entanglement preservation techniques.

Principle and experimental setup. - Figure 1(a) illustrates the process of entanglement purification. When many copies of entangled states are prepared, we can perform gates between two pairs of qubits, measure one pair, and post-select the remaining pair based on the measurement outcomes. For 2^N pairs of qubits with long coherence times, we can produce 2^{N-1} pairs by consuming half of the resource of low-quality entangled states. By repeating this process for all remaining pairs of qubits, we eventually obtain one pair of qubits with high-fidelity entanglement, at the cost of sacrificing the quantum resources of many low-fidelity entanglement pairs stored in the coupled qubits. However, this is not easily realized with current quantum systems because the generation of low-quality entanglement pairs is relatively slow, and the

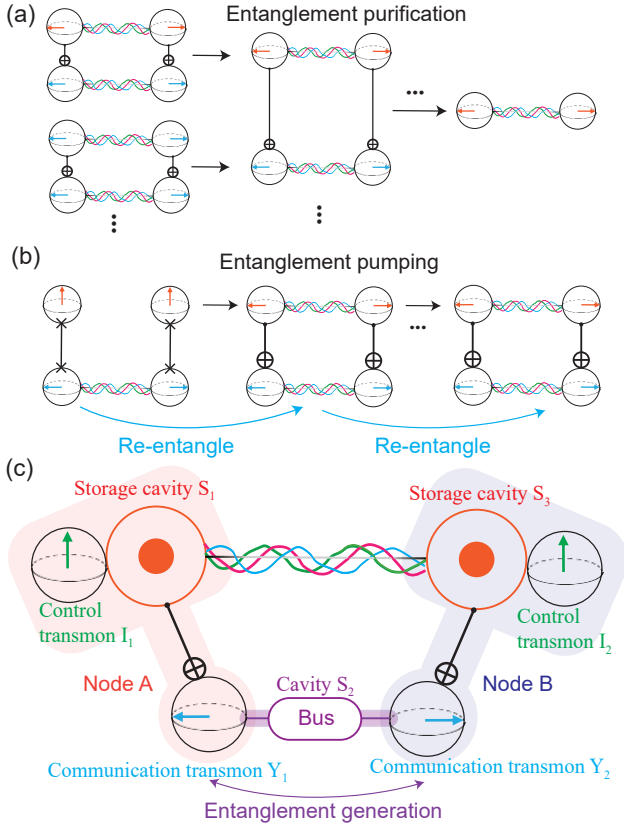


FIG. 1. Experimental device and principles for EP. (a) Schematic for entanglement purification. States from previous successful purification serve as inputs for the next round of purification. The total number of pairs increases exponentially with the number of rounds. (b) Schematic for EP. Entangled states are repeatedly generated on one pair of qubits and used to purify another pair. (c) Schematic of the experimental system. It contains three high-quality superconducting cavities and four transmon qubits.

available qubits are limited. Therefore, the relevant experimental demonstration remains a challenge.

Figure 1(b) shows a resource-efficient EP scheme for preparing quantum entangled states with only two pairs of qubits. One pair serves as communication qubits, which have relatively short coherence times but can couple to an intermediate bus waveguide or carriers to generate entanglement. In contrast, the other pair consists of qubits with long coherence times but lacks efficient channels for directly establishing entanglement. The high-quality qubits can serve as memory units, with their entanglement generated and sustained by repetitively pumping entanglement from the communication qubits. Since the communication qubits are reused during the process, there is no need for many pairs of communication qubits or long-coherence-time qubits.

We experimentally demonstrate EP within a superconducting quantum system. The schematic of our experimental device is shown in Fig. 1(c). Two 3D coaxial cavities (S_1 and S_3) serve as indirectly connected nodes (A and B) in the quantum network, aiming to store entangled quantum states. Each

cavity is coupled to a control transmon qubit (I_1 and I_2 , respectively), enabling arbitrary local operations on the cavities through numerically optimized pulses applied to both the cavities and the transmons [35–39]. The two cavities are interconnected by two communication transmon qubits (Y_1 and Y_2) and a bus cavity (S_2). With the assistance of bus resonator S_2 , entangled states can be repeatedly generated on the communication qubits Y_1 and Y_2 . Thus, we can utilize the regenerated entangled pairs to initialize and sustain the entanglement in the two storage cavities (S_1 and S_3).

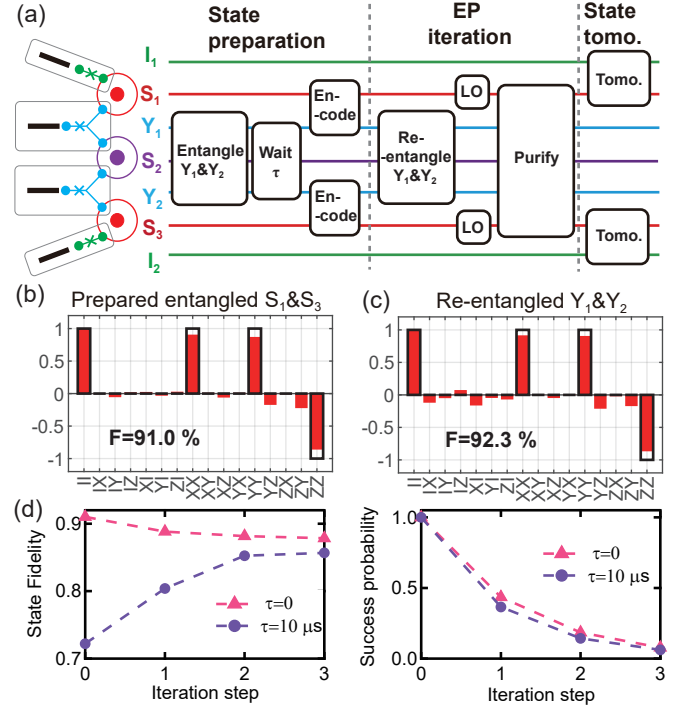


FIG. 2. Repetitive EP of physical qubits. (a) Experimental sequence for repetitive entanglement purification. (b) Prepared entangled state $|\psi\rangle = \frac{|01\rangle + |10\rangle}{\sqrt{2}}$ in cavities S_1 and S_3 for $\tau = 0$. (c) Re-entangled state in communication transmons Y_1 and Y_2 with an entangled photonic qubit state in cavities S_1 and S_3 . (d) The experimental results of continuous entanglement purification. Three rounds of non-local purification processes are performed.

EP for the physical qubits.— We begin by encoding quantum information into the two lowest photon number states, $|0\rangle$ and $|1\rangle$, of the storage cavities. Figure 2(a) shows the detailed experimental sequence. An initially entangled state $|\psi\rangle_+ = \frac{1}{\sqrt{2}}(|ge\rangle + |eg\rangle)$ is prepared between the communication qubits Y_1 and Y_2 , mediated by S_2 , and then encoded into the storage cavities S_1 and S_3 via local transmon-cavity swap operations at each node. Here, $|g\rangle$ and $|e\rangle$ represent the ground and excited states of the communication qubit, respectively. The entangled photonic qubits in S_1 and S_3 are characterized through state tomography using I_1 and I_2 . As shown in Fig. 2(b), the initial entangled photonic qubits exhibit a state fidelity of 91.0%. This entangled state is continuously pumped by repetitively regenerating entangled states

in Y_1 and Y_2 and performing the entanglement purification between the communication and photonic qubits. It is important to consider the dispersive coupling between the storage cavities and communication qubits when optimizing the control pulses for the re-entangling gate. The regenerated entanglement between the communication qubits achieves a fidelity of 92.3%, as shown in Fig. 2(c).

According to the entanglement purification schemes [40, 41], bilateral CNOT gates and post-selection of the communication qubit measurements in the $|gg\rangle$ state can effectively suppress unwanted components of $|\phi\rangle_{\pm} = \frac{1}{\sqrt{2}}(|00\rangle \pm |11\rangle)$ in the photonic qubit state. However, errors accumulate in the $|\psi\rangle_{-} = \frac{1}{\sqrt{2}}(|01\rangle - |10\rangle)$ state over multiple EP rounds, limiting the fidelity of the stored entangled state. To address this issue, we apply local single-qubit operations [42] to exchange the proportion of $|\psi\rangle_{-}$ with $|\phi\rangle_{\pm}$ before the CNOT gates. Both communication qubits are measured after the CNOT gates for post-selection. Ideally, we should keep the outputs when both communication qubits are in their ground states $|gg\rangle$ or excited states $|ee\rangle$. However, measuring the $|ee\rangle$ state causes an additional phase to the states in the storage cavities. Moreover, we have to reset the communication qubits to $|gg\rangle$ before the next pumping cycle, thus introducing additional errors. For simplicity, we discard $|ee\rangle$ events at the cost of reducing the success rate of purification in each round of EP by approximately half.

Figure 2(d) presents the evolution of entanglement state fidelity in the storage cavities during the repetitive EP process. When EP is performed directly without any extra wait time ($\tau = 0$), we find that the fidelity decreases with successive EP iterations and eventually saturates at a value of 87.8%. This behavior can be attributed to the accumulation of operation errors during the entanglement purification process and the use of imperfectly regenerated entanglement. Consequently, the steady-state achievable fidelity is limited by a balance of these imperfections, although the fidelity of the regenerated entanglement between the communication qubits is higher.

In contrast, by introducing a wait time of $\tau = 10 \mu\text{s}$ between EP iterations, which introduces errors in the storage cavities, we observe that EP can significantly improve the entanglement fidelity. Starting from an initial fidelity of 72.2%, the fidelity progressively increases with each EP round and ultimately reaches a saturation value of approximately 85.7%. This result confirms that the EP can effectively enhance and sustain improved entanglement fidelity when local memory decoherence is pronounced. Notably, the experiments demonstrate up to four rounds of EP, with the success probability of each round diminishing considerably as the number of iterations increases, revealing the trade-off between fidelity and resources. Numerical simulations and error budget analyses of the EP process can be found in Supplementary Materials [43].

Gate design for logical qubits. - To achieve longer coherence for stored entanglement, we can encode the states in the cavities using QEC codes. Here, we utilize the lowest-order binomial code to encode the logical qubits [44–47],

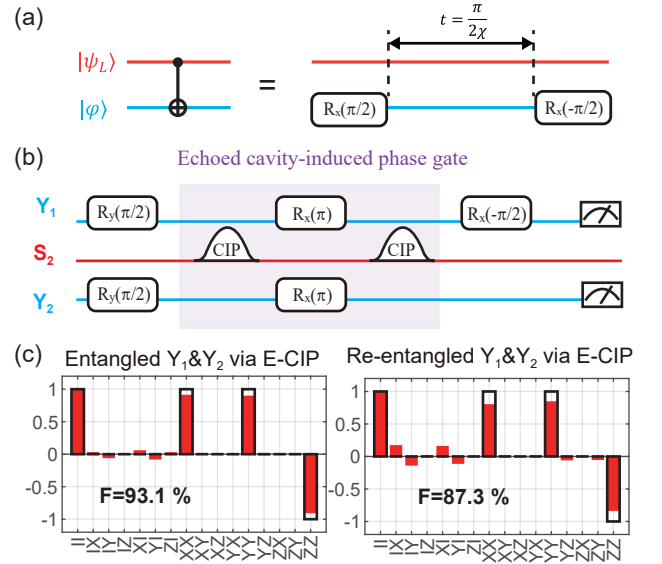


FIG. 3. Gate for purification of logical qubits. (a) Diagram for the CNOT gate between a binomial logical qubit and a communication qubit. (b) Experimental sequence for re-entangling communication qubits Y_1 and Y_2 using an echoed CIP gate. (c) Generated entangled state without (left) and with (right) a binomially entangled state in cavities S_1 and S_3 .

where the code space is spanned by $|0\rangle_L = (|0\rangle + |4\rangle)/\sqrt{2}$ and $|1\rangle_L = |2\rangle$. With this encoding, we can perform error detection for cavities S_1 and S_3 to mitigate the excitation loss errors in the memory. If a single-photon-loss error is indicated by the output of ED, the entangled logical qubits will be discarded. By combining ED with EP, high-quality ELQs can be prepared and sustained probabilistically, requiring only local operations on the cavities and control qubits in each node, along with classical communication between nodes.

For EP of logical qubits, two key challenges arise: the realization of the CNOT gate between the communication and logical qubits, and the high-fidelity re-entanglement between communication qubits in the presence of multiple photons in the storage cavities. To avoid the complex control pulses on a composite system of five subsystems ($S_{1,2,3}$ and $Y_{1,2}$), we develop two gates through simple controls. Figure 3(a) illustrates the scheme for the CNOT gate, which is decomposed into two Hadamard gates $R_x(\pi/2)$ and a controlled-Z (CZ) gate. The CZ gate between the logical and communication qubits can be realized using the dispersive coupling between them, which leads to the evolution operator $U = \exp(-i\chi a^\dagger a |e\rangle\langle e| T)$ with a gate duration of $T = \frac{\pi}{2\chi}$, where χ is the dispersive coupling strength.

Considering the dispersive coupling between the communication and logical qubits, we implement an echoed cavity-induced phase (CIP) gate to re-entangle the communication qubits. The mechanism of the CIP relies on the cavity-induced geometric phase to the qubits under external driving when they are dispersively coupled to a cavity [10–12]. For the two communication qubits dispersively coupled to

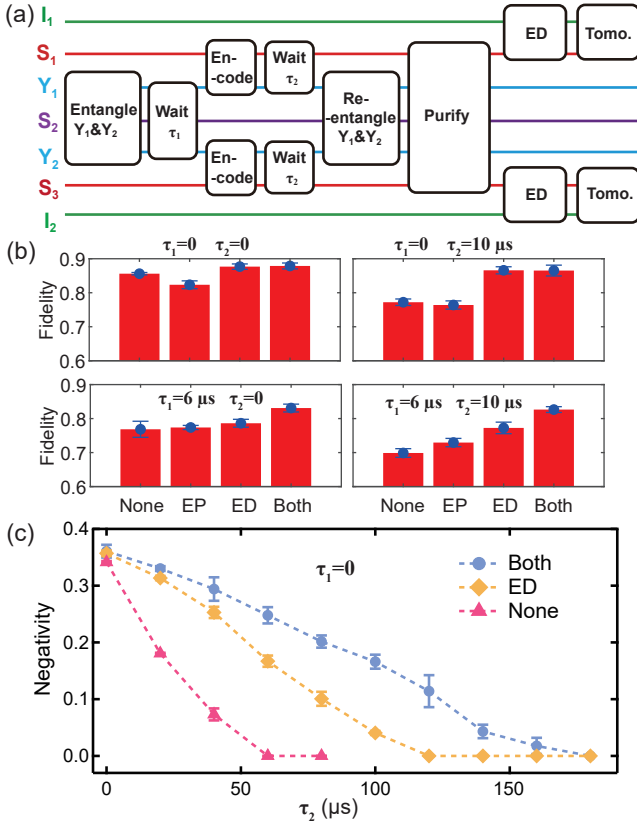


FIG. 4. The lifespan of ELQs through various purification schemes. (a) Experimental sequence for implementing both EP and ED. Wait times τ_1 and τ_2 are introduced to add logical errors and single-photon-loss errors, respectively. (b) State fidelity for scenarios with no purification, only EP, only ED, and the combination of both ED and EP under different wait times. (c) The influence of different purification schemes on the lifespan of ELQs. The negativity changes as a function of τ_2 with τ_1 set to 0.

S_2 , the Hamiltonian is given by $H_d = (\delta + \chi_{S_2 Y_1} |e\rangle\langle e|_{Y_1} + \chi_{S_2 Y_2} |e\rangle\langle e|_{Y_2}) \hat{a}_{S_2}^\dagger \hat{a}_{S_2}$, where a detuned drive (δ) on S_2 induces state-dependent geometric phases. Ideally, the CIP gate can convert the initial state of the communication qubits $|\psi_i\rangle = (|gg\rangle + |ge\rangle + |eg\rangle + |ee\rangle)/2$ to a final state $|\psi_f\rangle = (|ee\rangle + e^{i\Phi_1} |eg\rangle + e^{i\Phi_2} |ge\rangle + e^{i\Phi_3} |ee\rangle)/2$, with $\Phi_{1,2,3}$ being the corresponding phases.

To mitigate the influence of the dispersive couplings to cavities S_1 and S_3 , we employ an echoed CIP gate. As shown in Fig. 3(b), by inserting two flip operations $R_x(\pi)$ on the communication qubits between two identical CIP gates, the phases induced by the dispersive couplings with S_1 and S_3 are canceled out, and the converted final state becomes $|\psi_{f2}\rangle = (|gg\rangle + e^{i(\Phi_1 + \Phi_2 - \Phi_3)} |eg\rangle + e^{i(\Phi_1 + \Phi_2 - \Phi_3)} |ge\rangle + |ee\rangle)/2$. By carefully adjusting the duration of the CIP gates, we can satisfy the condition $\Phi_1 + \Phi_2 - \Phi_3 = \pi/2$, leading to the final state $|\psi_{f2}\rangle = [(|g\rangle + i|e\rangle)|g\rangle + (i|g\rangle + |e\rangle)|e\rangle]/2$. Finally, by applying a $R_x(-\pi/2)$ rotation to Y_1 , we obtain the target entangled state $|\psi_{f3}\rangle = (|eg\rangle + |ge\rangle)/\sqrt{2}$ on the communica-

tion qubits. The echoed CIP gate is characterized by state tomography under different conditions, with the results shown in Fig. 3(c) [see Supplementary Materials [43] for more details]. When both cavities S_1 and S_3 are in the vacuum state, the fidelity of the entangled communication qubits is 93.1%. When the cavities are prepared in the entangled binomial logical states, the fidelity decreases to 87.3%.

Combined EP and ED on logical qubits.- Equipped with the gates designed for logical qubits, we experimentally combine EP and ED methods to protect entanglement between two indirectly connected nodes. The experimental procedure, depicted in Fig. 4(a), incorporates two relaxation periods: τ_1 before encoding, which allows for the introduction of logical errors, and τ_2 after encoding, which enables the occurrence of correctable single-photon-loss errors. Figure 4(b) presents a comprehensive analysis of the fidelity improvements achieved through various EP and ED strategies under different error scenarios ($\tau_{1,2}$). In the absence of intentionally introduced errors ($\tau_1 = 0, \tau_2 = 0$), ED alone improves fidelity, primarily by mitigating single-photon-loss errors inherent to the first round of EP, which prepares the initial ELQs. Conversely, the EP iteration reduces fidelity. Interestingly, the simultaneous application of ED and EP yields a fidelity comparable to that obtained with ED alone. This can be attributed to the longer gate times associated with EP, which introduce additional single-photon-loss errors that can subsequently be compensated by ED.

When relaxation is introduced only after encoding ($\tau_1 = 0, \tau_2 = 10 \mu\text{s}$), single-photon loss becomes the dominant source of error. In this case, the changes in fidelity are similar to those observed when no errors are intentionally introduced. When relaxation is applied only before encoding ($\tau_1 = 6 \mu\text{s}, \tau_2 = 0$), the errors are mostly non-correctable. Thus, both ED and EP can independently enhance fidelity, with their combination leading to an even more pronounced improvement. Finally, the effects of EP and ED are most evident when relaxations are introduced both before and after the encoding stage ($\tau_1 = 6 \mu\text{s}, \tau_2 = 10 \mu\text{s}$).

To evaluate the potential of EP and ED on logical qubits in practical applications, we perform experiments without intentionally introducing relaxation before the encoding stage ($\tau_1 = 0$). Instead, we focus on extending the relaxation time τ_2 and characterize the preservation of entanglement by monitoring entanglement negativity \mathcal{N} [51]. The experimental results are depicted in Fig. 4(c), demonstrating enhanced preservation of entanglement when both ED and EP are applied, compared to the case with ED alone. Notably, the lifespan of ELQs increases by nearly 50%, extending from approximately $120 \mu\text{s}$ to $180 \mu\text{s}$.

Conclusion.- We have experimentally demonstrated the first realization of entanglement pumping on bosonic logical qubits encoded in superconducting cavities. By combining quantum error detection with non-local entanglement purification techniques, we provide a resource-efficient strategy for preserving and enhancing the fidelity of entangled states between indirectly connected nodes in a quantum network. By

reusing a pair of communication qubits and a pair of long-coherence storage cavities, we have demonstrated enhanced entanglement despite practical experimental imperfections, achieving a 50% increase in the lifespan of entangled logical qubits. Our results also highlight the potential of bosonic codes [28, 29] in quantum networks and provide new insights into entanglement management in modular quantum systems and distributed quantum information processing [30–34].

This work was funded by the National Natural Science Foundation of China (Grants No. 11925404, 92165209, 92365301, 12061131011, 92265210, 11890704, 92365206), Innovation Program for Quantum Science and Technology (Grant No. 2021ZD0300203 and 2021ZD0301800), and the National Key R&D Program (2017YFA0304303). This work was also supported by the Fundamental Research Funds for the Central Universities and USTC Research Funds of the Double First-Class Initiative. This work was partially carried out at the USTC Center for Micro and Nanoscale Research and Fabrication.

* These two authors contributed equally to this work.

† wangwt2020@tsinghua.edu.cn

‡ clzou321@ustc.edu.cn

§ luyansun@tsinghua.edu.cn

- [1] A. Einstein, B. Podolsky, and N. Rosen, “Can Quantum-Mechanical Description of Physical Reality Be Considered Complete?” *Physical Review* **47**, 777 (1935).
- [2] J. F. Clauser, M. A. Horne, A. Shimony, and R. A. Holt, “Proposed experiment to test local hidden-variable theories,” *Phys. Rev. Lett.* **23**, 880 (1969).
- [3] H. M. Hill, “Physics Nobel honors foundational quantum entanglement experiments,” *Physics Today* **75**, 14 (2022).
- [4] M. A. Nielsen and I. L. Chuang, *Quantum Computation and Quantum Information* (Cambridge Univ. Press, 2000).
- [5] C. H. Bennett, G. Brassard, C. Crépeau, R. Jozsa, A. Peres, and W. K. Wootters, “Teleporting an unknown quantum state via dual classical and einstein-podolsky-rosen channels,” *Phys. Rev. Lett.* **70**, 1895 (1993).
- [6] D. Bouwmeester, J.-W. Pan, K. Mattle, M. Eibl, H. Weinfurter, and A. Zeilinger, “Experimental quantum teleportation,” *Nature* **390**, 575 (1997).
- [7] X.-M. Hu, Y. Guo, B.-H. Liu, C.-F. Li, and G.-C. Guo, “Progress in quantum teleportation,” *Nature Reviews Physics* **5**, 339 (2023).
- [8] C. L. Degen, F. Reinhard, and P. Cappellaro, “Quantum sensing,” *Rev. Mod. Phys.* **89**, 035002 (2017).
- [9] S. Pirandola, B. R. Bardhan, T. Gehring, C. Weedbrook, and S. Lloyd, “Advances in photonic quantum sensing,” *Nat. Photonics* **12**, 724 (2018).
- [10] J. I. Cirac, P. Zoller, H. J. Kimble, and H. Mabuchi, “Quantum state transfer and entanglement distribution among distant nodes in a quantum network,” *Phys. Rev. Lett.* **78**, 3221 (1997).
- [11] H. J. Kimble, “The quantum internet,” *Nature* **453**, 1023 (2008).
- [12] A. Blais, A. L. Grimsmo, S. M. Girvin, and A. Wallraff, “Circuit quantum electrodynamics,” *Rev. Mod. Phys.* **93**, 025005 (2021).
- [13] W. Cai, X. Mu, W. Wang, J. Zhou, Y. Ma, X. Pan, Z. Hua, X. Liu, G. Xue, H. Yu, H. Wang, Y. Song, C.-L. Zou, and L. Sun, “Protecting entanglement between logical qubits via quantum error correction,” *Nature Physics* **20**, 1022 (2024).
- [14] W. Dür and H. J. Briegel, “Entanglement purification and quantum error correction,” *Reports on Progress in Physics* **70**, 1381 (2007).
- [15] L. Zhou and Y.-B. Sheng, “Purification of logic-qubit entanglement,” *Scientific Reports* **6**, 28813 (2016).
- [16] P.-S. Yan, L. Zhou, W. Zhong, and Y.-B. Sheng, “Advances in quantum entanglement purification,” *Sci. China Phys. Mech. Astron.* **66**, 250301 (2023).
- [17] X.-M. Hu, C.-X. Huang, Y.-B. Sheng, L. Zhou, B.-H. Liu, Y. Guo, C. Zhang, W.-B. Xing, Y.-F. Huang, C.-F. Li, and G.-C. Guo, “Long-distance entanglement purification for quantum communication,” *Phys. Rev. Lett.* **126**, 010503 (2021).
- [18] C.-X. Huang, X.-M. Hu, B.-H. Liu, L. Zhou, Y.-B. Sheng, C.-F. Li, and G.-C. Guo, “Experimental one-step deterministic polarization entanglement purification,” *Science Bulletin* **67**, 593 (2022).
- [19] P.-S. Yan, L. Zhou, W. Zhong, and Y.-B. Sheng, “Measurement-based logical qubit entanglement purification,” *Phys. Rev. A* **105**, 062418 (2022).
- [20] W. Dür, H.-J. Briegel, J. Cirac, and P. Zoller, “Quantum repeaters based on entanglement purification,” *Physical Review A* **59**, 169 (1999).
- [21] L. Childress, J. Taylor, A. Sørensen, and M. Lukin, “Fault-Tolerant Quantum Communication Based on Solid-State Photon Emitters,” *Physical Review Letters* **96**, 070504 (2006).
- [22] C. Wang, Y. Y. Gao, P. Reinhold, R. W. Heeres, N. Ofek, K. Chou, C. Axline, M. Reagor, J. Blumoff, K. M. Sliwa, L. Frunzio, S. M. Girvin, L. Jiang, M. Mirrahimi, M. H. Devoret, and R. J. Schoelkopf, “A Schrodinger cat living in two boxes,” *Science* **352**, 1087 (2016).
- [23] S. Rosenblum, Y. Y. Gao, P. Reinhold, C. Wang, C. J. Axline, L. Frunzio, S. M. Girvin, L. Jiang, M. Mirrahimi, M. H. Devoret, and R. J. Schoelkopf, “A CNOT gate between multiphoton qubits encoded in two cavities,” *Nat. Commun.* **9**, 652 (2018).
- [24] K. S. Chou, J. Z. Blumoff, C. S. Wang, P. C. Reinhold, C. J. Axline, Y. Y. Gao, L. Frunzio, M. H. Devoret, L. Jiang, and R. J. Schoelkopf, “Deterministic teleportation of a quantum gate between two logical qubits,” *Nature* **561**, 368 (2018).
- [25] A. Erhard, H. Poulsen Nautrup, M. Meth, L. Postler, R. Stricker, M. Stadler, V. Negnevitsky, M. Ringbauer, P. Schindler, H. J. Briegel, R. Blatt, N. Friis, and T. Monz, “Entangling logical qubits with lattice surgery,” *Nature* **589**, 220 (2021).
- [26] C. Ryan-Anderson, N. C. Brown, M. S. Allman, B. Arkin, G. Asa-Attuah, C. Baldwin, J. Berg, J. G. Bohnet, S. Braxton, N. Burdick, J. P. Campora, A. Chernoguzov, J. Esposito, B. Evans, D. Francois, J. P. Gaebler, T. M. Gatterman, J. Gerber, K. Gilmore, D. Gresh, A. Hall, A. Hankin, J. Hostetter, D. Lucchetti, K. Mayer, J. Myers, B. Neyenhuis, J. Santiago, J. Sedlacek, T. Skripka, A. Slattery, R. P. Stutz, J. Tait, R. Tobey, G. Vittorini, J. Walker, and D. Hayes, “Implementing fault-tolerant entangling gates on the five-qubit code and the color code,” *arXiv: 2208.01863* (2022).
- [27] L. Jiang, J. M. Taylor, A. S. Sørensen, and M. D. Lukin, “Scalable quantum networks based on few-qubit registers,” *International Journal of Quantum Information* **08**, 93 (2010).
- [28] W. Cai, Y. Ma, W. Wang, C.-L. Zou, and L. Sun, “Bosonic quantum error correction codes in superconducting quantum circuits,” *Fundamental Research* **1**, 50 (2021).
- [29] A. Joshi, K. Noh, and Y. Y. Gao, “Quantum information processing with bosonic qubits in circuit qed,” *Quantum Science*

- and *Technology* **6**, 033001 (2021).
- [30] J. I. Cirac, A. K. Ekert, S. F. Huelga, and C. Macchiavello, “Distributed quantum computation over noisy channels,” *Physical Review A* **59**, 4249 (1999).
- [31] A. S. Cacciapuoti, M. Caleffi, F. Tafuri, F. S. Cataliotti, S. Gherardini, and G. Bianchi, “Quantum Internet: Networking Challenges in Distributed Quantum Computing,” *IEEE Network* **34**, 137 (2020).
- [32] L. Jiang, J. M. Taylor, A. S. Sørensen, and M. D. Lukin, “Distributed quantum computation based on small quantum registers,” *Phys. Rev. A* **76**, 062323 (2007).
- [33] C. Monroe, R. Raussendorf, A. Ruthven, K. R. Brown, P. Maunz, L.-M. Duan, and J. Kim, “Large-scale modular quantum-computer architecture with atomic memory and photonic interconnects,” *Phys. Rev. A* **89**, 022317 (2014).
- [34] D. Awschalom, K. K. Berggren, H. Bernien, S. Bhave, L. D. Carr, P. Davids, S. E. Economou, D. Englund, A. Faraon, M. Fejer, S. Guha, M. V. Gustafsson, E. Hu, L. Jiang, J. Kim, B. Kozh, P. Kumar, P. G. Kwiat, M. Lončar, M. D. Lukin, D. A. Miller, C. Monroe, S. W. Nam, P. Narang, J. S. Orcutt, M. G. Raymer, A. H. Safavi-Naeini, M. Spiropulu, K. Srinivasan, S. Sun, J. Vučković, E. Waks, R. Walsworth, A. M. Weiner, and Z. Zhang, “Development of quantum interconnects (quics) for next-generation information technologies,” *PRX Quantum* **2**, 017002 (2021).
- [35] R. W. Heeres, P. Reinhold, N. Ofek, L. Frunzio, L. Jiang, M. H. Devoret, and R. J. Schoelkopf, “Implementing a universal gate set on a logical qubit encoded in an oscillator,” *Nature Communications* **8**, 94 (2017).
- [36] N. Khaneja, T. Reiss, C. Kehlet, T. Schulte-Herbrüggen, and S. J. Glaser, “Optimal control of coupled spin dynamics: design of nmr pulse sequences by gradient ascent algorithms,” *Journal of Magnetic Resonance* **172**, 296 (2005).
- [37] S. Krastanov, V. V. Albert, C. Shen, C.-L. Zou, R. W. Heeres, B. Vlastakis, R. J. Schoelkopf, and L. Jiang, “Universal control of an oscillator with dispersive coupling to a qubit,” *Physical Review A* **92** (2015), 10.1103/PhysRevA.92.040303.
- [38] R. W. Heeres, B. Vlastakis, E. Holland, S. Krastanov, V. V. Albert, L. Frunzio, L. Jiang, and R. J. Schoelkopf, “Cavity state manipulation using photon-number selective phase gates,” *Phys. Rev. Lett.* **115**, 137002 (2015).
- [39] A. Eickbusch, V. Sivak, A. Z. Ding, S. S. Elder, S. R. Jha, J. Venkatraman, B. Royer, S. M. Girvin, R. J. Schoelkopf, and M. H. Devoret, “Fast universal control of an oscillator with weak dispersive coupling to a qubit,” *Nature Physics* **18**, 1464 (2022).
- [40] C. H. Bennett, G. Brassard, S. Popescu, B. Schumacher, J. A. Smolin, and W. K. Wootters, “Purification of noisy entanglement and faithful teleportation via noisy channels,” *Phys. Rev. Lett.* **76**, 722 (1996).
- [41] C. H. Bennett, D. P. DiVincenzo, J. A. Smolin, and W. K. Wootters, “Mixed-state entanglement and quantum error correction,” *Phys. Rev. A* **54**, 3824 (1996).
- [42] D. Deutsch, A. Ekert, R. Jozsa, C. Macchiavello, S. Popescu, and A. Sanpera, “Quantum privacy amplification and the security of quantum cryptography over noisy channels,” *Phys. Rev. Lett.* **77**, 2818 (1996).
- [43] “See Supplementary Materials.”
- [44] M. H. Michael, M. Silveri, R. T. Brierley, V. V. Albert, J. Salmilehto, L. Jiang, and S. M. Girvin, “New class of quantum error-correcting codes for a bosonic mode,” *Phys. Rev. X* **6**, 031006 (2016).
- [45] L. Hu, Y. Ma, W. Cai, X. Mu, Y. Xu, W. Wang, Y. Wu, H. Wang, Y. P. Song, C. L. Zou, S. M. Girvin, L. M. Duan, and L. Sun, “Quantum error correction and universal gate set operation on a binomial bosonic logical qubit,” *Nature Physics* **15**, 503 (2019).
- [46] Y. Ma, Y. Xu, X. Mu, W. Cai, L. Hu, W. Wang, X. Pan, H. Wang, Y. P. Song, C. L. Zou, and L. Sun, “Error-transparent operations on a logical qubit protected by quantum error correction,” *Nature Physics* **16**, 827 (2020).
- [47] Z. Ni, S. Li, X. Deng, Y. Cai, L. Zhang, W. Wang, Z.-B. Yang, H. Yu, F. Yan, S. Liu, C.-L. Zou, L. Sun, S.-B. Zheng, Y. Xu, and D. Yu, “Beating the break-even point with a discrete-variable-encoded logical qubit,” *Nature* **616**, 56 (2023).
- [10] D. Dong, Y.-L. Zhang, C.-L. Zou, X.-B. Zou, and G.-C. Guo, “Quantum phase gate through the dispersive atom-field interaction with atoms trapped in optical cavity qed,” *Physics Letters A* **379**, 2291 (2015).
- [11] S. Puri and A. Blais, “High-fidelity resonator-induced phase gate with single-mode squeezing,” *Phys. Rev. Lett.* **116**, 180501 (2016).
- [12] H. Paik, A. Mezzacapo, M. Sandberg, D. T. McClure, B. Abdo, A. D. Córcoles, O. Dial, D. F. Bogorin, B. L. T. Plourde, M. Steffen, A. W. Cross, J. M. Gambetta, and J. M. Chow, “Experimental demonstration of a resonator-induced phase gate in a multiqubit circuit-qed system,” *Phys. Rev. Lett.* **117**, 250502 (2016).
- [51] G. Vidal and R. F. Werner, “Computable measure of entanglement,” *Phys. Rev. A* **65**, 032314 (2002).

Supplementary Materials

I. EXPERIMENT SETUP AND SYSTEM PARAMETERS

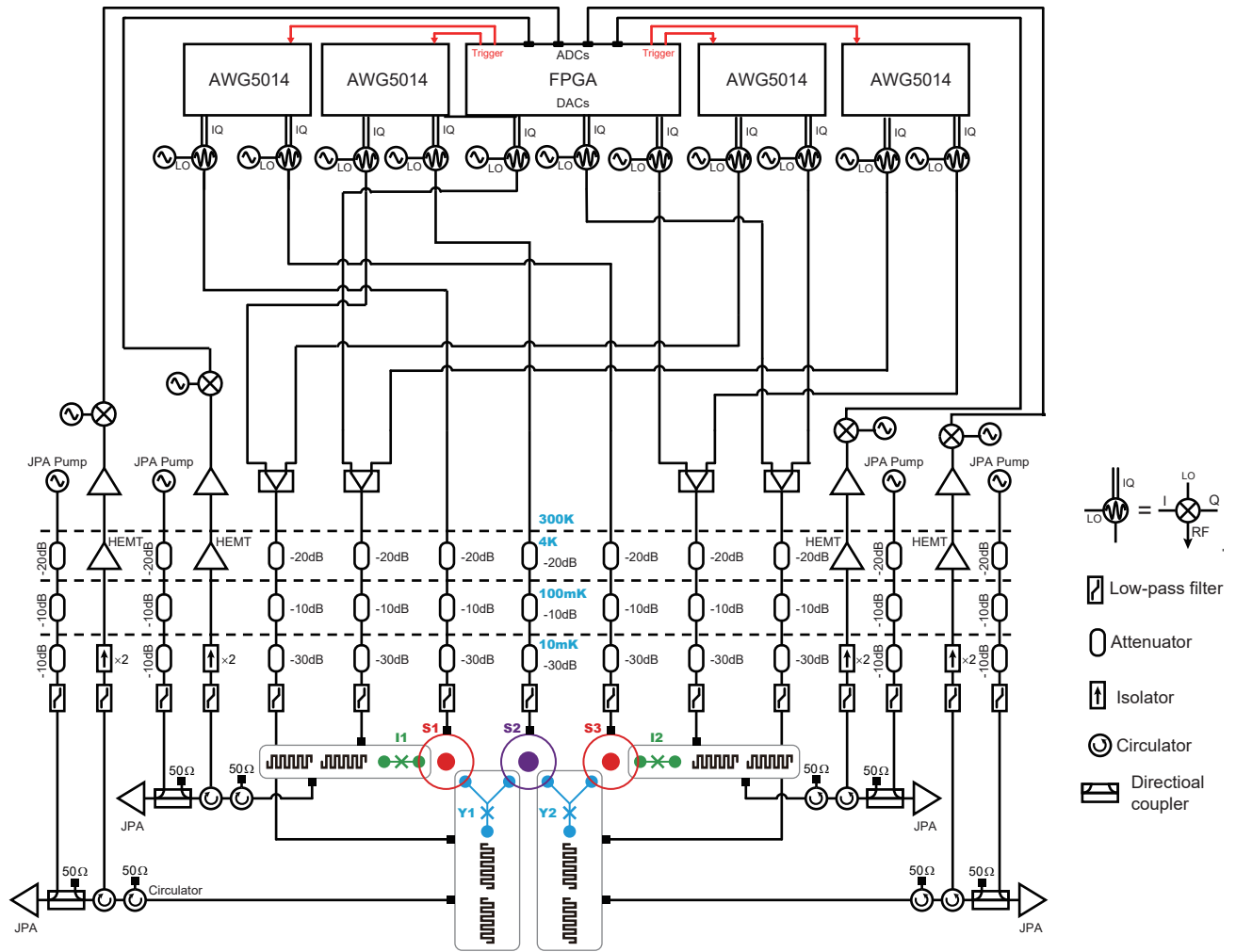
Our experiment utilizes two high-Q superconducting cavities (S_1 and S_3) to store entangled quantum states, each coupled to an I -type transmon (I_1 and I_2 , respectively) that serves as a control qubit for manipulation. These two cavities are interconnected via two Y -type transmons (Y_1 and Y_2) functioning as communication qubits, along with another superconducting cavity (S_2).

The detailed system wiring is shown in Fig. S1. The device is placed on the base plate of a dilution refrigerator with a temperature of approximately 10 mK. All modes mentioned above are controlled by signals generated through an IQ mixing process, with the IQ signals produced by either arbitrary waveform generators (AWG) or the digital-to-analog converter (DAC) ports of field programmable gate arrays (FPGA). The output signals are amplified by Josephson parametric amplifiers (JPA) [1, 2], together with high-electron mobility transistors at 4 K.

The dynamics of our system can be described by the Hamiltonian

$$H = \sum_i K_i \hat{a}_i^\dagger \hat{a}_i^\dagger \hat{a}_i \hat{a}_i + \sum_{i \neq j} \chi_{ij} \hat{a}_i^\dagger \hat{a}_i \hat{a}_j^\dagger \hat{a}_j, \quad (\text{S1})$$

with $i, j \in \{S_1, S_2, S_3, I_1, I_2, Y_1, Y_2\}$. Here K_i is the strength of the self-Kerr term of mode i , χ_{ij} is the cross-Kerr coupling strength between modes i and j , and \hat{a}_i is the annihilation operator of mode i . Table I shows the measured nonlinear coupling strength in Eq. S1. The coherence times and thermal populations for each mode are also measured in experiment, and the results are shown in Table II.



Supplementary Figure S1. **The system wiring.** All input control signals are generated through an IQ mixing process. All the microwave lines are appropriately attenuated and filtered at different stages.

Supplementary Table I. The measured nonlinear interactions ($\chi_{ij}/2\pi$ in MHz) of the system (— means the term is not measurable; \sim means this term is not measured.)

Mode	I_1	S_1	Y_1	S_2	Y_2	S_3	I_2
I_1	\sim	1.329	0.003	—	0.005	—	—
S_1	1.329	0.003	0.655	< 0.001	—	—	—
Y_1	0.003	0.655	\sim	1.433	0.023	—	—
S_2	—	< 0.001	1.433	0.004	0.711	< 0.001	—
Y_2	0.005	—	0.023	0.711	\sim	0.475	0.027
S_3	—	—	—	< 0.001	0.475	0.002	1.411
I_2	—	—	—	—	0.027	1.411	\sim

Supplementary Table II. The measured resonant mode frequencies, coherence times, and thermal populations.

Mode	Frequency (GHz)	T_1 (μ s)	T_2^* (μ s)	n_{th}
I_1	4.232	80-110	30-70	3.5%
S_1	6.102	261	—	3%
Y_1	5.045	50-80	20-40	1%
S_2	5.561	258	—	2%
Y_2	4.707	80-120	70-100	3%
S_3	6.006	256	—	2.5%
I_2	4.479	65-85	40-70	4%

II. ENTANGLEMENT PUMPING

A. Principle

The details of the protocol of entanglement pumping (EP) can be found in Reference [3]. For completeness, we explain the key principles in this section, starting with the basic entanglement purification protocol. Suppose we have two entangled pairs, with fidelities F_A and F_B , respectively. For simplicity, we assume that the states are depolarized Werner state [4], meaning that their density matrices can be written as:

$$\begin{aligned}\rho_A &= F_A |\psi_+\rangle \langle \psi_+| + \frac{1-F_A}{3} (|\psi_-\rangle \langle \psi_-| + |\phi_+\rangle \langle \phi_+| + |\phi_-\rangle \langle \phi_-|), \\ \rho_B &= F_B |\psi_+\rangle \langle \psi_+| + \frac{1-F_B}{3} (|\psi_-\rangle \langle \psi_-| + |\phi_+\rangle \langle \phi_+| + |\phi_-\rangle \langle \phi_-|),\end{aligned}\quad (\text{S2})$$

where $|\psi_+\rangle = \frac{|01\rangle + |10\rangle}{\sqrt{2}}$, $|\psi_-\rangle = \frac{|01\rangle - |10\rangle}{\sqrt{2}}$, $|\phi_+\rangle = \frac{|00\rangle + |11\rangle}{\sqrt{2}}$, and $|\phi_-\rangle = \frac{|00\rangle - |11\rangle}{\sqrt{2}}$. Here, $|0\rangle$ and $|1\rangle$ represent the two basis states of the qubits. If we want to increase the fidelity of the entangled pair labeled as A, we can use the two qubits in party A as control qubits and apply CNOT operations to the two qubits in party B, as shown in Fig. S2(a).

Afterward, we measure the two qubits in party B, and retain the quantum states in party A if the measurement results are the same. The fidelity of the entangled pair that is retained in party A will then become

$$F' = \frac{F_A F_B + \left(\frac{1-F_A}{3}\right)\left(\frac{1-F_B}{3}\right)}{F_A F_B + F_A \left(\frac{1-F_B}{3}\right) + \left(\frac{1-F_A}{3}\right) F_B + 5\left(\frac{1-F_A}{3}\right)\left(\frac{1-F_B}{3}\right)}. \quad (\text{S3})$$

For a given F_B , there exists an upper limit F_{limit} for purification. If $F_A < F_{\text{limit}}$, the fidelity of the entangled state in party A will increase after purification; if $F_A > F_{\text{limit}}$, the fidelity will decrease after purification. Making $F' = F_A$, we can solve Eq. S3 and get the fidelity limit:

$$F_{\text{limit}} = \frac{3(2F_B - 1) + \sqrt{28F_B^2 - 26F_B + 7}}{2(4F_B - 1)}. \quad (\text{S4})$$

We plot the curve of F_{limit} in Fig. S2(b). The re-entangled fidelity realized in our experiment (92.3%) is indicated in the figure by a gray arrow, and the corresponding $F_{\text{limit}} = 95.8\%$.

The basic idea of EP is to repeatedly generate entangled states in party B and use them to purify the entangled state in party A over and over again. If any purification step fails, we need to start over the entire process. Although this method sacrifices the success probability, it can always push the fidelity of the entangled state from a smaller value to F_{limit} .

However, it should be noted that during the EP process, the entangled state in party A will gradually deviates from the depolarized Werner state, and errors will accumulate in $|\psi^-\rangle \langle \psi^-|$ subspace. This is caused by two reasons. First, the entanglement purification process increases not only the proportion of $|\psi^+\rangle \langle \psi^+|$ but also the proportion of $|\psi^-\rangle \langle \psi^-|$. Second, single-qubit dephasing errors may convert state $|\psi^+\rangle$

to $|\psi^-\rangle$. When the proportion of $|\psi^-\rangle \langle \psi^-|$ is too large, purification will no longer improve, and may even reduce the fidelity of the entangled state. Therefore, we need to perform local operations to stop the accumulation of errors. In our experiment, we employ the DEJMPS protocol [5]. After every purification step, we perform an $R_x(\frac{\pi}{2})$ transformation on cavity S_1 and an $R_x(-\frac{\pi}{2})$ transformation on cavity S_3 . After the transformations, the proportions of $|\psi^-\rangle \langle \psi^-|$ and $|\phi^-\rangle \langle \phi^-|$ are swapped. As a result, the proportions of all three kinds of error states can be reduced continuously.

B. Gates optimized by GRAPE

As discussed in the main text, in order to realize EP, we need several quantum gates including two-qubit (Y_1 and Y_2) entanglement and re-entanglement gates, encode-decode gates, CNOT gates between cavities and transmon qubits, and local operation gates on cavities. In our experiment, all these gates are realized via numerical optimization using the gradient ascent pulse engineering method (GRAPE) [6, 7]. The communication qubit entanglement gates and encode-decode gates have been introduced in previous works [8]. In this section, we will mainly discuss the implementation of the re-entanglement gates, CNOT gates, and local operations.

The goal of the re-entanglement gate is to regenerate entanglement on the communication qubits Y_1 and Y_2 under the condition that an entangled state already exists between the storage cavities S_1 and S_3 . Since the coupling between the cavity and the qubit cannot be turned off, the entanglement gate optimized by considering only the modes Y_1 , Y_2 , and S_2 will no longer function properly. Therefore, when optimizing the re-entanglement gate, we need to take into account all five modes: Y_1 , Y_2 , S_1 , S_2 , and S_3 .

For optimization, we define the initial state $|\psi_i\rangle$ and the target state $|\psi_t\rangle$ as constraints. For the regular entanglement gate, when both S_1 and S_3 are in their vacuum states, the constraints are given by

$$\begin{aligned}|\psi_i\rangle &= (|g\rangle |0\rangle |g\rangle)_{Y_1 S_2 Y_2}, \\ |\psi_t\rangle &= \frac{1}{\sqrt{2}} (|g\rangle |0\rangle |e\rangle + |e\rangle |0\rangle |g\rangle)_{Y_1 S_2 Y_2},\end{aligned}\quad (\text{S5})$$

where $|g\rangle$ and $|e\rangle$ represent the ground and excited states of the communication qubits, and $|0\rangle$ stands for the vacuum state of cavity S_2 . For the re-entanglement gate, when S_1 and S_3 are encoded in $\{|0\rangle, |1\rangle\}$, the constraints become

$$\begin{aligned}|\psi_i\rangle &= \frac{1}{\sqrt{2}} (|0\rangle |1\rangle + |1\rangle |0\rangle)_{S_1 S_3} \otimes (|g\rangle |0\rangle |g\rangle)_{Y_1 S_2 Y_2}, \\ |\psi_t\rangle &= \frac{1}{2} (|0\rangle |1\rangle + |1\rangle |0\rangle)_{S_1 S_3} \otimes (|g\rangle |0\rangle |e\rangle + |e\rangle |0\rangle |g\rangle)_{Y_1 S_2 Y_2}.\end{aligned}\quad (\text{S6})$$

It is worth noting that for both of the above gates, the drives are applied only to the modes Y_1 , S_2 , and Y_2 . Therefore, we can truncate S_1 and S_3 to the first two levels. As a result, the dimension of the time evolution operators become 16 times the

Supplementary Table III. Error budgets of our experiment. F_i and x_i are the fidelity and depolarizing ratio, respectively, for the corresponding error type.

error type	F_i	x_i
Re-entangle	0.961	0.948
Qubit decoherence	0.944	0.925
Cavity decay	0.974	0.965
All error	0.882	0.843
experiment	0.867	0.823

original size, which is acceptable in numerical computation. However, for binomial encoding, the truncation extends to the first five energy levels, and the computational dimension increases to 625 times the original size, which is unacceptable. Therefore, we employ the echoed cavity-induced phase (CIP) gate to realize re-entanglement gate for the entangled logical qubits (ELQ) in the storage cavities, as described in the main text.

As for the CNOT gates and the local operations, both of them only involve two modes: $S_{1(3)}$ and $Y_{1(2)}$. Therefore, they can be relatively easily optimized. For simplicity, we have combined these two operations into a single unitary for optimization, which can be expressed as $U = U_{\text{local}}U_{\text{CNOT}}$.

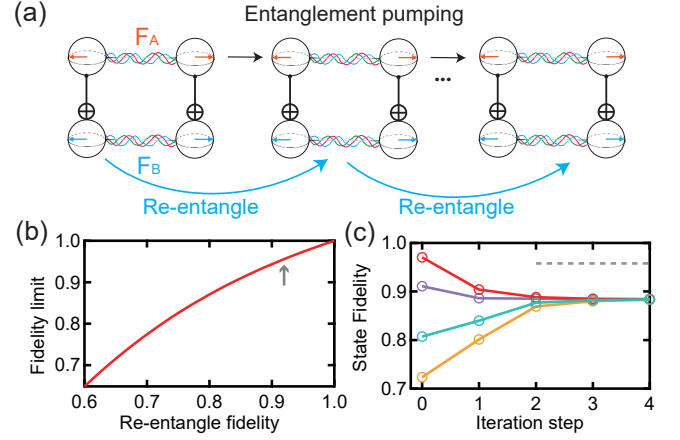
C. Numerical simulation

As described above, EP can increase the fidelity of the entangled state to F_{limit} with ideal operations. However, due to factors such as qubit decoherence and measurement errors, the actual converged fidelity will always be lower than F_{limit} . To assess the impact of decoherence on the final fidelity, we carry out numerical simulations [9] of the EP process with the parameters in Tables I and II and the experimentally measured density matrix of the re-entangled state.

The simulation results are shown in Fig. S2(c). We choose four Werner states with different fidelities as the initial states. After three rounds of EP, their fidelities all converge to around 88.2%, which is 7.6% lower than the ideal fidelity limit (shown as dashed line). The data presented in the main text, however, converge to around 86.7%, which is only slightly lower than the simulation results. This indicates that the final fidelity is primarily limited by decoherence. The difference between simulation and experiment could be attributed to errors not included in the simulation, such as measurement errors for post-selection.

To further quantify the contributions of cavity decay and qubit decoherence to the final fidelity, we conduct additional analysis. Since we have performed the local operations, the final steady state can be approximately considered as a depolarized Werner state:

$$\rho_f = x|\psi_+\rangle\langle\psi_+| + \frac{1-x}{4}\hat{I}, \quad (\text{S7})$$



Supplementary Figure S2. Upper bound of the EP fidelity and simulation results. (a) Schematic of the EP protocol. (b) Theoretical limit of the converged fidelity for the purified entangled state varies with the re-entangled state fidelity. The measured re-entangled state fidelity (92.3%) is marked by the array. (c) Simulation results of the EP process for different initial states. We adopt the measured re-entangled state and include the decoherence of the communication qubits and cavities during the CNOT gates and local operations. The theoretical upper bound of the converged fidelity is indicated by the dashed line.

where x is the depolarizing ratio. It should be noted that Eq. S2 and Eq. S7 are two equivalent representations, and the ratio x and state fidelity F satisfy $x = \frac{4F-1}{3}$. Assuming that the effects of various errors on the final fidelity are independent, the ratio x can be expressed as

$$x = \prod_i x_i, \quad (\text{S8})$$

where i represents different types of errors. To extract the ratio corresponding to each type of error, we add only the specific type of errors in simulation, obtain the final converged fidelity, and convert it into x_i .

The simulation results are shown in Table III. The data in the row labeled as ‘‘re-entangle’’ is obtained from simulation with experimentally measured re-entangled density matrix and ideal operations. The resulting fidelity is very close to the theoretically predicted upper limit (0.958), and the difference is likely due to the simulation precision. From the data in Table III, we can see that qubit decoherence contributes the most to the infidelity. If we multiply x_i of the first three rows, we obtain $\prod_i x_i = 0.846$, which aligns to the one obtained from the simulation with all errors included (0.843). This justifies the assumption of independent errors.

III. ECHOED CAVITY-INDUCED PHASE GATE

In the main text, we briefly discuss the basic idea of echoed CIP gate. In this section, we will provide more information about the principle of CIP gate and the calibration experiment.

A. Principle of CIP gate

The basic idea of the CIP gate is that by adiabatically turning on and off off-resonant drives, the state in the cavity traverses a qubit-state-dependent closed path in phase space [10–12], as shown in Fig. S3. After this process, the cavity returns to the vacuum state, while different qubit states accumulate nontrivial phases.

When we apply an off-resonant drive to cavity S_2 , the Hamiltonian of the $Y_1 - S_2 - Y_2$ system in the rotating frame of the drive can be expressed as

$$\hat{H} = (\delta + \frac{1}{2}\chi_1\hat{\sigma}_{Z_1} + \frac{1}{2}\chi_2\hat{\sigma}_{Z_2})\hat{a}_{S_2}^\dagger\hat{a}_{S_2} + \varepsilon(t)(\hat{a}_{S_2}^\dagger + \hat{a}_{S_2}), \quad (\text{S9})$$

where $\delta = \omega_{S_2} - \omega_d$, $\varepsilon(t)$ is the time-dependent drive amplitude, $\chi_{1(2)}$ is the dispersive coupling strength between the communication qubit $Y_{1(2)}$ and cavity S_2 , $\hat{\sigma}_{Z_1}$ ($\hat{\sigma}_{Z_2}$) is the Pauli-Z operator for the communication qubit, and \hat{a}_{S_2} ($\hat{a}_{S_2}^\dagger$) is the annihilation (creation) operator for cavity S_2 .

To get the effective two-qubit interaction Hamiltonian, we follow the derivation in Reference [11]. We apply a time-dependent displacement to transform $\hat{H}_{\text{eff}} = D(\hat{\alpha}')^\dagger\hat{H}D(\hat{\alpha}') - iD(\hat{\alpha}')^\dagger\dot{D}(\hat{\alpha}')$ to Hamiltonian S9. Here, $D(\hat{\alpha}') = \exp(\hat{\alpha}'\hat{a}^\dagger - \hat{\alpha}'^*\hat{a})$ and $\hat{\alpha}' = \alpha(1 - \frac{\chi_1\hat{\sigma}_{Z_1} + \chi_2\hat{\sigma}_{Z_2}}{2\delta})$, where $\dot{\alpha} = -i\delta - i\varepsilon(t)$. We can get the effective Hamiltonian:

$$\hat{H}_{\text{eff}} = \delta\hat{a}_{S_2}^\dagger\hat{a}_{S_2} + \frac{1}{2}(\chi_1\hat{\sigma}_{Z_1} + \chi_2\hat{\sigma}_{Z_2})(\hat{a}_{S_2}^\dagger\hat{a}_{S_2} + |\alpha|^2) - \frac{\chi_1\chi_2|\alpha|^2}{2\delta}\hat{\sigma}_{Z_1}\hat{\sigma}_{Z_2}. \quad (\text{S10})$$

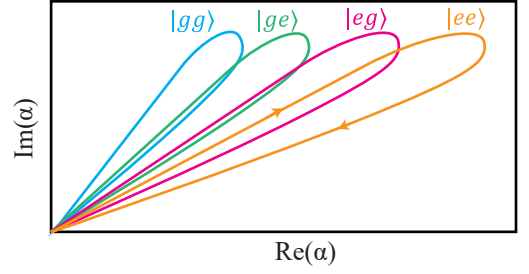
The nontrivial two-qubit phase originates from the last term of Hamiltonian S10, and the rate of phase accumulation is proportional to $|\alpha|^2/\delta$. To ensure the adiabaticity of the process, we set a Gaussian profile for the CIP gate used in the experiment, defined as

$$\varepsilon(t) = A\exp(-\frac{8(t - \tau/2)^2}{\tau^2}). \quad (\text{S11})$$

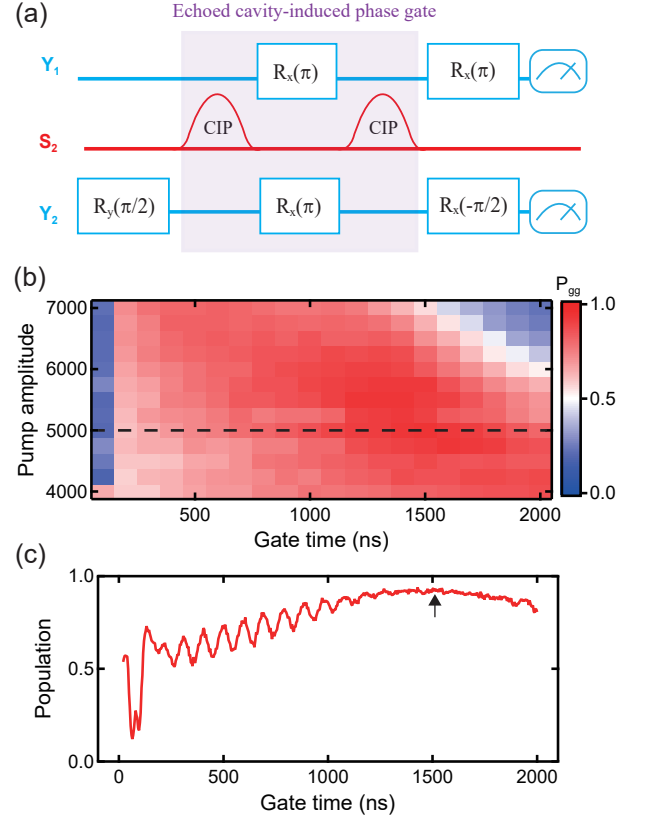
Here, A is the maximum pump amplitude and τ is the total gate time. From Eq. S10 and Eq. S11, we can get $|\tilde{\alpha}| \propto A/\delta$, and the rate of phase accumulation is then proportional to A^2/δ^3 . As a result, the total gate time $\tau \propto \delta^3/A^2$. Therefore, to shorten the gate time, we can either increase the pump amplitude A or reduce δ . However, it is important to note that an excessively large pump amplitude or a small detuning may destroy the adiabatic process, preventing the cavity from returning to the vacuum state.

B. Calibration of echoed CIP gate

The superposition state of the two communication qubits Y_1 and Y_2 , $|\psi_i\rangle = (|gg\rangle + |ge\rangle + |eg\rangle + |ee\rangle)/2$ will evolve into $|\psi_f\rangle = (|gg\rangle + e^{i(\Phi_1 + \Phi_2 - \Phi_3)}|eg\rangle + e^{i(\Phi_1 + \Phi_2 - \Phi_3)}|ge\rangle +$



Supplementary Figure S3. **Diagram for the CIP gate.** The state of the storage cavity adiabatically evolves along a qubit-state-dependent loop in phase space. As a result, the two communication qubits acquire a nontrivial phase and become entangled.



Supplementary Figure S4. **Experimental sequence and results for the calibration of the echoed CIP gate.** (a) Experimental sequence for calibrating the echoed CIP gate. (b) Population of $|gg\rangle$ varies with the gate time (single CIP gate) and pump amplitude, with $\delta/2\pi = 10$ MHz. (c) Linecut of (b) at the position indicated by the black dashed line. The gate time used in the experiment is indicated by the black array.

$|ee\rangle)/2$ after the echoed CIP gate. To prepare the maximally entangled state, we need to satisfy the condition $\Phi_1 + \Phi_2 - \Phi_3 = \pi/2$.

To determine the gate time required to meet such a condition, we design the experiment shown in Fig. S4(a). First, we prepare a superposition state on qubit Y_2 using an $R_y(\frac{\pi}{2})$ rota-

tion pulse, and the joint state on Y_1 and Y_2 can be expressed as $|\psi_0\rangle = \frac{1}{\sqrt{2}}(|gg\rangle + |ge\rangle)$. Next, we implement the echoed CIP gate, and $|\psi_0\rangle$ will undergo the following evolution:

$$\begin{aligned} |\psi_0\rangle &= \frac{1}{\sqrt{2}}(|gg\rangle + |ge\rangle) \\ \xrightarrow{\text{CIP}} |\psi_1\rangle &= \frac{1}{\sqrt{2}}(|gg\rangle + e^{i\Phi_1}|ge\rangle) \\ \xrightarrow{\text{Echo}} |\psi_2\rangle &= \frac{1}{\sqrt{2}}(|ee\rangle + e^{i\Phi_1}|eg\rangle) \\ \xrightarrow{\text{CIP}} |\psi_3\rangle &= \frac{1}{\sqrt{2}}(e^{i\Phi_3}|ee\rangle + e^{i(\Phi_1+\Phi_2)}|eg\rangle). \end{aligned} \quad (\text{S12})$$

Finally, we apply an $R_x(\pi)$ rotation to qubit Y_1 and an $R_x(-\frac{\pi}{2})$ rotation to qubit Y_2 . When $\Phi_1 + \Phi_2 - \Phi_3 = \pi/2$, the state will come back to the ground state $|gg\rangle$. Conversely, if $\phi_1 + \phi_2 - \phi_3 \neq \pi/2$, the qubit state will not fully return to the ground state. In the experiment, we can scan the gate time, and the position that maximizes the population of $|gg\rangle$ corresponds to the required time.

Figure S4(b) shows the measured population of $|gg\rangle$ (P_{gg}) as a function of pump amplitude and gate time with $\delta/2\pi = 10$ MHz. Figure S4(c) shows the linecut of Fig. S4(b) at the pump amplitude of $A = 5000$. Here, the gate time represents the time of a single CIP gate. The data in Fig. S4(c) indicate a gate time of $\tau = 1500$ ns, where P_{gg} reaches its maximum value. It is noted that when the gate time is too short, P_{gg} exhibits significant oscillations due to the rapid change rate of ϵ , which breaks the adiabatic approximation.

To ensure that the parameters ($\delta/2\pi = 10$ MHz, $A = 5000$, $\tau = 1500$ ns) do not result in excessive residual photons in S_2 , we perform a numerical simulation following the sequence shown in Fig. 3(b) of the main text, using the deco-

herence parameters in Table II. The simulation results show that after the entire echoed CIP gate, the photon number in S_2 does not exceed 1%. This confirms that these parameters satisfy the adiabatic condition well, and we finally adopt them for the experiment.

* These two authors contributed equally to this work.

† wangwt2020@tsinghua.edu.cn

‡ clzou321@ustc.edu.cn

§ luyansun@tsinghua.edu.cn

- [1] T. Roy, S. Kundu, M. Chand, A. M. Vadiraj, A. Ranadive, N. Nehra, M. P. Patankar, J. Aumentado, A. A. Clerk, and R. Vijay, *Applied Physics Letters* **107**, 262601 (2015).
- [2] A. Kamal, A. Marblestone, and M. Devoret, *Phys. Rev. B* **79**, 184301 (2009).
- [3] W. Dür and H. J. Briegel, *Reports on Progress in Physics* **70**, 1381 (2007).
- [4] R. F. Werner, *Phys. Rev. A* **40**, 4277 (1989).
- [5] D. Deutsch, A. Ekert, R. Jozsa, C. Macchiavello, S. Popescu, and A. Sanpera, *Phys. Rev. Lett.* **77**, 2818 (1996).
- [6] N. Khaneja, T. Reiss, C. Kehlet, T. Schulte-Herbrüggen, and S. J. Glaser, *J. Magn. Reson.* **172**, 296 (2005).
- [7] P. de Fouquieres, S. Schirmer, S. Glaser, and I. Kuprov, *J. Magn. Reson.* **212**, 412 (2011).
- [8] W. Cai, X. Mu, W. Wang, J. Zhou, Y. Ma, X. Pan, Z. Hua, X. Liu, G. Xue, H. Yu, H. Wang, Y. Song, C.-L. Zou, and L. Sun, *Nature Physics* (2024), 10.1038/s41567-024-02446-8.
- [9] J. R. Johansson, P. D. Nation, and F. Nori, *Computer Physics Communications* **184**, 1234 (2013).
- [10] D. Dong, Y.-L. Zhang, C.-L. Zou, X.-B. Zou, and G.-C. Guo, *Physics Letters A* **379**, 2291 (2015).
- [11] S. Puri and A. Blais, *Phys. Rev. Lett.* **116**, 180501 (2016).
- [12] H. Paik, A. Mezzacapo, M. Sandberg, D. T. McClure, B. Abdo, A. D. Córcoles, O. Dial, D. F. Bogorin, B. L. T. Plourde, M. Steffen, A. W. Cross, J. M. Gambetta, and J. M. Chow, *Phys. Rev. Lett.* **117**, 250502 (2016).